Synthesis and Antibacterial Activity of Peptide Deformylase Inhibitors†

Kristi M. Huntington,‡ Tian Yi,‡ Yaoming Wei, and Dehua Pei*

Department of Chemistry and Ohio State Biochemistry Program, The Ohio State University, 100 West 18th Avenue, Columbus, Ohio 43210

Received October 21, 1999; Revised Manuscript Received January 31, 2000

ABSTRACT: Peptide deformylase catalyzes the removal of the N-terminal formyl group from newly synthesized polypeptides in eubacteria. Its essential character in bacterial cells makes it an attractive target for antibacterial drug design. In this work, we have rationally designed and synthesized a series of peptide thiols that act as potent, reversible inhibitors of purified recombinant peptide deformylase from *Escherichia coli* and *Bacillus subtilis*. The most potent inhibitor has a K_I value of 11 nM toward the *B. subtilis* enzyme. These inhibitors showed antibacterial activity against both Gram-positive and Gram-negative bacteria, with minimal inhibitory concentrations (MIC) as low as 5 μM (∼2 μg/mL). The PDF inhibitors induce bacterial cell lysis and are bactericidal toward all four bacterial strains that have been tested, *B. subtilis*, *Staphylococcus epidermidis*, *Enterococcus faecalis*, and *E. coli*. Resistance evaluation of one of the inhibitors (**1b**) against *B. subtilis* showed that no resistant clone could be found from $>1 \times 10^9$ cells. Quantitative analysis using a set of inhibitors designed to possess varying potencies against the deformylase enzyme revealed a linear correlation between the MIC values and the K_I values. These results suggest that peptide deformylase is the likely molecular target responsible for the antibacterial activity of these inhibitors and is therefore a viable target for antibacterial drug design.

The emergence of bacterial pathogens that are resistant to multiple classes of existing antibiotics has created an urgent demand for new antibacterial agents with novel mechanisms of action (*1*−*4*). Recent genetic studies have suggested that peptide deformylase (PDF)[1] may be a suitable target for antibacterial drug design (*5*, *6*). In bacteria, protein synthesis starts with an *N*-formylmethionine, and as a result, all newly synthesized polypeptides carry transiently a formylated N-terminus (*7*). PDF catalyzes the subsequent removal of the formyl group from the majority of those polypeptides, many of which undergo further N-terminal processing by methionine aminopeptidase to produce mature proteins (*8*). As an essential activity for survival (*5*, *6*), PDF is present in all eubacteria. Since protein synthesis in the eukaryotic cytoplasm does not involve the formyl group and PDF is apparently absent in higher eukaryotes, including man (*9*), PDF inhibitors are expected to act as a new class of broad-spectrum antibacterial agents.

PDF is a unique metallopeptidase, which utilizes a ferrous ion (Fe^{2+}) to catalyze the amide bond hydrolysis (*9*−*11*). The extreme sensitivity of the Fe^{2+} ion to environmental oxygen renders PDF one of the most unstable enzymes known and has prevented its characterization for three decades (*12*−*15*). We and others have recently replaced the ferrous ion with Zn^{2+} (*9*, *10*, *16*), Ni^{2+} (*11*, *17*), and Co^{2+} (*18*). While substitution of Zn^{2+} reduces the activity by over 2 orders of magnitude, the Ni(II)- and Co(II)-substituted PDF forms retain almost full catalytic activity of the native enzyme. The metal-substituted PDF forms are highly stable, permitting detailed biochemical and structural characterization of this enzyme. X-ray crystallographic and nuclear magnetic resonance studies of the Co^{2+}, Zn^{2+}, Ni^{2+}, and Fe^{2+} PDF forms reveal virtually identical three-dimensional structures (*19*−*24*). The metal ion is tetrahedrally coordinated by a water molecule and the side chains of two histidines of the conserved HExxH motif and of a conserved cysteine. Catalysis is mediated by the nucleophilic attack on the substrate carbonyl group by a metal-bound hydroxide (*18*, *23*, *24*). The glutamate side chain in the conserved HExxH motif serves as a general acid, protonating the departing amide ion during the decomposition of the tetrahedral intermediate (*18*).

In this work, we report the *first* synthesis and evaluation of a series of peptide thiols as potent metal-chelating inhibitors of *Escherichia coli* and *Bacillus subtilis* PDF. The most potent inhibitor exhibits reversible binding to the PDF with inhibition constants (K_I) in the low nanomolar range. These inhibitors show potent antibacterial activity toward Gram-positive bacteria and moderate activity against Gram-negative bacteria.

MATERIALS AND METHODS

General. *N*-Fluorenylmethoxycarbonyl- (Fmoc-) protected amino acids (**6a** and **6b**) were from Advanced ChemTech (Louisville, KY). Leucyl-*p*-nitroanilide (**7a**) was from Sigma Chemical Co. Tris(2-carboxyethyl)phosphine hydrochloride

† This work was supported by a grant from the National Institutes of Health (AI40575).

* Corresponding author: Department of Chemistry, The Ohio State University, 100 W. 18th Ave., Columbus, OH 43210. Telephone (614) 688-4068; Fax (614) 292-1532; E-mail pei.3@osu.edu.

‡ These two authors contributed equally to this work.

[1] Abbreviations: PDF, peptide deformylase; f-ML-*p*NA, *N*-formylmethionylleucyl-*p*-nitroanilide; MIC, minimum inhibitory concentration; AAP, *Aeromonas* aminopeptidase; TFA, trifluoroacetic acid; Fmoc, *N*-fluorenylmethoxycarbonyl; PCLNA, (S)-2-*O*-(*H*-phosphonoxy)-L-caproyl-L-leucyl-*p*-nitroanilide; TCEP, tris(2-carboxyethyl)phosphine.

10.1021/bi992452y CCC: $19.00
Published on Web 03/16/2000

(TCEP) was purchased from Pierce. All other chemicals were from Aldrich. Native PDF (Fe−PDF) and Co(II)-substituted PDF (Co−PDF) of *Escherichia coli* were purified as described (*15*, *18*). *Bacillus subtilis*, *Staphylococcus epidermidis*, and *Enterococcus faecalis* strains were kindly provided by Dr. Neil Baker of The Ohio State University. ^{1}H NMR spectra were recorded on Bruker spectrometers at the indicated field strength and chemical shifts are given as parts per million (ppm) relative to the internal standard, tetramethylsilane. Mass spectroscopic analysis was performed at The Ohio State University Campus Chemical Instrument Center.

Purification of B. subtilis Co−PDF. *B. subtilis def* gene (*25*) was cloned by a polymerase chain reaction (PCR) using two primers, 5′-GGGGATCCATATGGCAGTAAAAAAG-GTCGT-3′ and 5′-GGGAATTCACTCGAGTCCTTCCAT-ATCCGCTAGT-3′, and *B. subtilis* chromosomal DNA as template. The PCR conditions were the same as those described for the cloning of the *E. coli* PDF (*10*). The PCR product (∼500 bp) was digested with *Nde*I and *Eco*RI endonucleases and cloned into plasmid pET-22b (Novagen). *E. coli* BL21(DE3) cells transformed with the overproducing plasmid were grown in minimal medium to $OD_{600} = 0.8$ and induced by the addition of 100 μM isopropyl β-D-thiogalactopyranoside and 100 μM $CoCl_2$ for 18 h (*18*). The cells were collected by centrifugation and lysed by lysozyme as described (*18*). The crude lysate was fractionated on a Q-Sepharose column (2.5 × 15 cm) by eluting with 20 mM Tris·HCl (pH 8.5) plus a linear gradient of 10−500 mM NaCl. The resulting PDF was of ∼95% purity and was stored at −80 °C.

General Procedure for the Synthesis of 2-Alkylacrylic Acids (**4a**−**f**). 2-Alkylacrylic acids **4a**−**f** were prepared from dimethyl malonate according to a literature procedure (*26*−*29*). Dimethyl malonate (44 mmol) and sodium methoxide (88 mmol) in methanol (100 mL) were refluxed for 20 min and the proper alkyl iodide (30 mmol) in methanol (50 mL) was added. The reaction was refluxed for 20 min and then cooled to room temperature, and the solvent was evaporated under vacuum. The residue was distributed into 50 mL of diethyl ether saturated with NH_4Cl and the ether layer was collected, concentrated, and purified on a silica gel column (eluted with ethyl acetate/hexane, 1:3) to afford dimethyl 2-alkylmalonates **2a**−**f** in 11−62% yields. **2a** (R = *n*-butyl): ^{1}H NMR (200 MHz, $CDCl_3$) δ 3.71 (s, 6 H), 3.34 (t, J = 7.5 Hz, 1 H), 1.80−1.97 (m, 2 H), 1.15−1.45 (m, 4 H), 0.87 (t, 3 H). **2b** (R = isobutyl): ^{1}H NMR (200 MHz, $CDCl_3$) δ 3.73 (s, 6H), 3.45 (t, J = 7.6 Hz, 1 H), 1.80 (t, J = 7.4 Hz, 2 H), 1.40−1.68 (m, 1 H), 0.91 (d, J = 6.5 Hz, 6 H). Compounds **2c**−**f** were directly used in the following reactions without characterization.

A solution of dimethyl 2-alkylmalonate **2a**−**f** (10 mmol) and NaOH (0.88 g, 22 mmol) in 30 mL of 1:1 (v/v) H_2O/MeOH was refluxed for 1 h. After being cooled to room temperature, the reaction solution was diluted with H_2O (30 mL) and extracted with ethyl acetate (30 mL). The aqueous layer was cooled to 0 °C, acidified to pH = 1 with concentrated hydrochloric acid, and extracted with ethyl acetate (3 × 20 mL). The combined organic layer was dried with $MgSO_4$ and the solvent was evaporated to give 2-alkylmalonic acids (**3a**−**f**) as white solids.

Each acid **3a**−**f** from above was dissolved in 20 mL of ethyl acetate and cooled to 0 °C when dimethylamine (20 mmol) and paraformaldehyde (15 mmol) were added. The reaction was stirred at room temperature for 10 min and then refluxed for 2 h, after which the initial suspension became a homogeneous solution. The reaction mixture was cooled to room temperature and 30 mL of H_2O was added. After cooling to 0 °C, the solution was acidified to pH = 1 with concentrated hydrochloric acid and extracted with ethyl acetate (2 × 30 mL). The combined organic phase was dried with $MgSO_4$ and the solvent was evaporated to give the desired products **4a**−**f**. The yields were 45−95% for two steps. 2-(*n*-Butyl)acrylic acid (**4a**): ^{1}H NMR (300 MHz, $CDCl_3$): δ 6.28 (s, 1 H), 5.64 (s, 1 H), 2.31 (t, J = 7.5 Hz, 2 H), 1.22−1.58 (m, 4 H), 0.92 (t, J = 7.2 Hz, 3 H). 2-Isobutylacrylic acid (**4b**): ^{1}H NMR (200 MHz, $CDCl_3$): δ 6.32 (s, 1 H), 5.61 (s, 1 H), 2.17 (d, J = 7.0 Hz, 2 H), 1.70−1.97 (m, 1 H), 0.89 (d, J = 6.6 Hz, 6 H). 2-Benzylacrylic acid (**4c**): ^{1}H NMR (200 MHz, $CDCl_3$): δ 7.12−7.60 (m, 5 H), 6.38 (s, 1 H), 5.58 (s, 1 H), 3.63 (s, 2 H). Compounds **4d**−**f** were used directly in the next step without characterization.

General Procedure for the Synthesis of 3-(S-Acetyl)-mercapto-2-alkylpropionic Acids (**5a**−**f**). Acids **5a**−**f** were prepared by modifying a literature procedure (*26*−*29*). 2-Alkylacrylic acid (**4a**−**f**) (10 mmol) was mixed with thiolacetic acid (15 mmol). The mixture was refluxed for 2 h and cooled to room temperature. The excess thiolacetic acid was evaporated under vacuum to give the products in quantitative yields. To remove the trace impurities derived from commercial thiolacetic acid samples, the products were dissolved in 50 mL of 5% $NaHCO_3$ solution and extracted with ethyl acetate (2 × 50 mL). The aqueous layer was cooled to 0 °C, carefully acidified to pH = 2 with concentrated hydrochloric acid, and extracted with ethyl acetate (50 mL). The ethyl acetate layer was dried with $MgSO_4$ and the solvent was evaporated to give the pure products. 3-(*S*-Acetyl)mercapto-2-(*n*-butyl)propionic acid (**5a**). ^{1}H NMR (200 MHz, $CDCl_3$) δ 2.95−3.20 (m, 2 H), 2.52−2.70 (m, 1 H), 2.33 (s, 3 H), 1.52−1.80 (m, 2 H), 1.20−1.45 (m, 4 H), 0.89 (t, J = 6.6 Hz, 3 H). 3-(*S*-Acetyl)-mercapto-2-isobutylpropionic acid (**5b**): ^{1}H NMR (200 MHz, $CDCl_3$) δ 2.87−3.23 (m, 2 H), 2.57−2.78 (m, 1 H), 2.34 (s, 3 H), 1.52−1.83 (m, 2 H), 1.28−1.50 (m, 1 H), 0.93 (d, J = 6.6 Hz, 6 H). 3-(*S*-Acetyl)mercapto-2-benzylpropionic acid (**5c**). ^{1}H NMR (200 MHz, $CDCl_3$) δ 7.10−7.40 (m, 5 H), 2.80−3.20 (m, 5 H), 2.33 (s, 3 H). 3-(*S*-Acetyl)mercapto-2-propylpropionic acid (**5d**): ^{1}H NMR (400 MHz, $CDCl_3$) δ 3.15 (dd, J = 8.2 and 5.4 Hz, 1 H), 3.03 (dd, J = 8.6 and 5.0 Hz, 1 H), 2.64 (m, 1 H), 2.34 (s, 3 H), 1.69 (m, 1 H), 1.60 (m, 1 H), 1.42 (m, 2 H), 0.94 (t, J = 7.3 Hz, 3 H). 3-(*S*-Acetyl)mercapto-2-ethylpropionic acid (**5e**): ^{1}H NMR (250 MHz, $CDCl_3$) δ 10.08 (br s, 1 H), 3.11 (dd, J = 7.9 and 5.8 Hz, 1 H), 3.05 (dd, J = 8.3 and 3.9 Hz, 1 H), 2.20 (s, 3 H), 1.57 (m, 2 H), 0.86 (t, J = 7.4 Hz, 3 H). 3-(*S*-Acetyl)mercapto-2-methylpropionic acid (**5f**): ^{1}H NMR (200 MHz, $CDCl_3$) δ 2.95−3.20 (m, 2 H), 2.60−2.85 (m, 1 H), 2.33 (s, 3 H), 1.28 (d, J = 7.1 Hz, 3 H).

N^{ϵ}-Boc-L-lysyl-p-nitroanilide (**7b**). Phosphorus oxychloride (3.4 mmol) was added dropwise to a solution of *p*-nitroaniline (0.27 g, 2.1 mmol), N^{α}-Fmoc-L-Lys(Boc) (1.0 g, 2.1 mmol), and imidazole (0.29 g, 3.4 mmol) in pyridine (10 mL) at 0 °C under argon. The mixture was stirred at room temperature for 3 h and the reaction solution was poured into 100 mL of

sodium bicarbonate solution. The mixture was extracted with ethyl acetate (3 × 50 mL) and the combined organic layer was washed with 30 mL each of a $CuSO_4$ solution and brine and dried over $MgSO_4$. After removal of the solvent, the crude product was purified by flash chromatography on a silica gel column to give 0.92 g (76%) of a white solid. ^{1}H NMR (300 MHz, $CDCl_3$): δ 9.11 (s, 1 H), 8.16 (d, J = 9.3 Hz, 2 H), 7.75 (d, J = 7.8 Hz, 2 H), 7.71 (d, J = 9.3 Hz, 2 H), 7.57 (d, J = 7.5 Hz, 2 H), 7.28 (t, J = 7.5 Hz, 2 H), 7.27 (t, J = 7.5 Hz, 2 H), 5.60 (s, 1 H), 4.71 (m, 1 H), 4.45 (d, J = 7.2 Hz, 2 H), 4.30 (s, 1 H), 4.21 (d, J = 6.9 Hz, 1 H), 3.23 (m, 1 H), 3.09 (m, 1 H), 1.73 (m, 2 H), 1.55 (m, 4 H), 1.44 (s, 9 H).

The white solid from above (600 mg) was dissolved in 10 mL of 20% piperidine in dichloromethane and the solution was stirred for 1 h at room temperature. Evaporation of the solvent and silica gel chromatography gave 0.30 g of product (**7b**) as a yellow oil (81% yield). ^{1}H NMR (300 MHz, $CDCl_3$): δ 10.01 (s, 1 H), 8.20 (d, J = 7.2 Hz, 2 H), 7.77 (d, J = 7.26 Hz, 2 H), 4.58 (s, 1 H), 3.50 (m, 1 H), 3.13 (m, 2 H), 1.98 (m, 2 H), 1.57 (m, 4 H), 1.43 (s, 9 H). *N*$^{\epsilon}$-Boc-L-lysylanilide (**7c**) was prepared in the same manner as **7b**.

N-[α-(Mercaptomethyl)caproyl]-L-lysyl-p-nitroanilide (**1b**). Dicyclohexylcarbodiimide (40 mg, 0.20 mmol) was added to a solution of **7b** (60 mg, 0.16 mmol) and **5a** (40 mg, 0.20 mmol) in 10 mL of dichloromethane. After stirring for 4 h at room temperature, the mixture was filtered to remove the white precipitate formed. The filtrate was concentrated and purified by silica gel chromatography to give 40 mg of a yellow solid (compound **8b**, 44% yield). ^{1}H NMR (400 MHz, $CDCl_3$): δ 9.56 (s, 1 H), 8.08 (m, 2 H), 7.6 (m, 2 H), 6.73 (s, 1 H), 2.38 (m, 1 H), 2.17 (s, 3 H), 1.87 (m, 2 H), 1.65 (m, 2 H), 1.47 (m, 2 H), 1.36 (s, 9 H), 1.23 (m, 6 H), 0.82 (m, 3 H).

Compound **8b** (0.40 g, 0.72 mmol) was dissolved in 10 mL of ethanol and sodium borohydride (100 mg, 2.63 mmol) was added. The mixture was stirred for 6 h at room temperature and 1.0 mL of water plus a few drops of 5% HCl were added to quench the reaction. The solvent was evaporated and the residue was dissolved in 20 mL of ethyl acetate. The solution was washed with brine, dried over $MgSO_4$, and concentrated to give a yellow solid. This yellow solid was dissolved in 20 mL of dichloromethane and 3 mL of trifluoroacetic acid (TFA) was added to the solution. The mixture was stirred for 5 h at room temperature. The solvent was evaporated and the residue was triturated with diethyl ether to give 0.20 g of **1b** as a yellow solid (53% yield in two steps). ^{1}H NMR (250 MHz, CD_3COCD_3): δ 8.08 (m, 2 H), 7.83 (m, 2 H), 4.48 (m, 1 H), 3.73 (m, 2 H), 3.27 (m, 1 H), 3.16 (m, 1 H), 2.61 (m, 1 H), 1.70−1.85 (m, 2 H), 1.40−1.60 (m, 6 H), 1.15−1.25 (m, 5 H), 0.98 (t, J = 7.0 Hz, 3 H). FAB-MS: *m*/*z* (relative intensity) 411.16 (100), 819.23 (50) (disulfide dimer). ESI−HRMS calcd for $C_{19}H_{31}N_4O_4S^+$, 411.2061; found, 411.2037.

N-[α-(Mercaptomethyl)caproyl]-L-leucyl-p-nitroanilide (**1a**). This compound was prepared from **5a** and leucyl-*p*-nitroanilide (**7a**) in a manner similar to **1b** except that no TFA treatment was necessary. ^{1}H NMR (300 MHz, $CDCl_3$): δ 9.56 and 9.61 (s, 1 H), 8.00−8.15 (m, 2 H), 7.50−7.70 (m, 2 H), 6.31 and 6.25 (d, J = 7.6 Hz, 1 H), 4.60−4.80 (m, 1 H), 2.52−2.90 (m, 2 H), 2.28−2.50 (m, 1 H), 1.43−1.94 (m, 6 H), 1.13−1.43 (m, 4 H), 0.65−1.08 (m, 9 H). FAB-MS: calcd for $C_{19}H_{30}N_3O_4S^+$, 396.1952; found *m*/*z* (relative intensity) 396.18 (65), 339.15 (22), and 258.18 (100).

N-[(2-Isobutyl-3-mercapto)propionyl]-L-lysyl-p-nitroanilide (**1c**). This compound was prepared in a similar manner as **1b**. ^{1}H NMR (400 MHz, CD_3COCD_3): δ 10.22 (m, 1 H), 8.01 (m, 2 H), 7.74 (m, 2 H), 5.70 (br s, 2 H), 4.51 (m, 1 H), 3.71 (m, 2 H), 3.04 (m, 1 H), 2.30−2.60 (m, 2 H), 1.70−1.90 (m, 4 H), 1.45−1.70 (m, 6 H), 0.70−0.90 (m, 6 H). FAB-MS: *m*/*z* (relative intensity) 411. 17 (100), 819.24 (12) (disulfide dimer). ESI−HRMS calcd for $C_{19}H_{31}N_4O_4S^+$ 411.2061, found 411.2087.

N-[(2-Benzyl-3-mercapto)propionyl]-L-lysyl-p-nitroanilide (**1d**). This compound was prepared in a similar manner as **1b**. ^{1}H NMR (250 MHz, CD_3COCD_3): δ 9.94 (s, 1 H), 8.03−8.08 (m, 2 H), 7.70−7.85 (m, 2 H), 6.90−7.15 (m, 5 H), 5.59 (s, 2 H), 4.30−4.50 (m, 1 H), 3.50−3.70 (m, 2 H), 2.60−2.90 (m, 3 H), 2.35−2.55 (m, 2 H), 1.40−1.80 (m, 7 H). FAB-MS: *m*/*z* (relative intensity) 445.18 (100). ESI−HRMS calcd for $C_{22}H_{29}N_4O_4S^+$, 445.1904; found, 445.1887.

N-[(2-Mercaptomethyl)valeryl]-L-lysyl-p-nitroanilide (**1e**). This compound was prepared in a similar manner as **1b**. ^{1}H NMR (250 MHz, CD_3COCD_3) δ 8.07 (m, 2 H), 7.81 (m, 2 H), 4.48 (m, 1 H), 3.72 (m, 2 H), 2.50−2.70 (m, 1 H), 2.45 (m, H), 1.70−1.90 (m, 4 H), 1.40−1.60 (m, 5 H), 1.15−1.25 (m, 2 H), 0.75 (m, 3 H). FAB-MS: *m*/*z* (relative intensity) 397.18 (100), 791.53 (12) (disulfide dimer). ESI−HRMS calcd for $C_{18}H_{29}N_4O_4S^+$, 397.1904; found, 397.1900.

N-[(2-Mercaptomethyl)-n-butyryl]-L-lysyl-p-nitroanilide (**1f**). This compound was prepared in a similar manner as **1b**. ^{1}H NMR (250 MHz, CD_3COCD_3) δ 8.08 (d, J = 7.5 Hz, 2 H), 7.81 (d, J = 7.5 Hz, 2 H), 4.84 (br s, 2 H), 4.47 (m, 1 H), 3.72 (m, 2 H), 2.55 (m, 1 H), 2.45 (m, 2 H), 1.70−1.85 (m, 4 H), 1.40−1.60 (m, 5 H), 0.77 (m, 3 H). FAB-MS: *m*/*z* (relative intensity) 383.23 (100). ESI−HRMS calcd for $C_{17}H_{27}N_4O_4S^+$ 383.1749, found 383.1728.

N-[(3-Mercapto-2-methyl)propionyl]-L-lysyl-p-nitroanilide (**1g**). This compound was prepared in a manner similar to **1b**. ^{1}H NMR (250 MHz, CD_3COCD_3): δ 8.04 (m, 2 H), 7.85 (m, 2 H), 4.47 (m, 1 H), 3.71 (m, 2 H), 3.10−3.40 (m, 2 H), 2.62 (m, 1 H), 1.70−1.90 (m, 4 H), 1.40−1.60 (m, 3 H), 1.03 (m, 3 H). FAB-MS: *m*/*z* (relative intensity) 490.12 (42), 431.33 (100), 409.15 (74), 369.13 (20). ESI−HRMS calcd for $C_{16}H_{25}N_4O_4S^+$, 369.1591; found, 369.1544.

N-[(α-Mercaptomethyl)caproyl]-L-lysylanilide (**1h**). This compound was prepared in a similar manner as **1b** from **5a** and **7c**. ^{1}H NMR (250 MHz, $CDCl_3$): δ 7.56 (m, 2 H), 7.11 (m, 2 H), 6.92 (m, 1 H), 4.40−4.65 (m, 1 H), 2.80−2.90 (m, 2 H), 2.45−2.65 (m, 2 H), 1.95−2.10 (m, 1 H), 1.67−1.87 (m, 4 H), 1.40−1.60 (m, 4 H), 1.10−1.30 (m, 4 H), 0.70−0.80 (m, 3 H). FAB-MS: *m*/*z* (relative intensity) 729.35 (31) (disulfide dimer), 608.22 (52), 593.34 (72), 526.25 (100), 390.13 (34), 366.14 (12). ESI−HRMS calcd for $C_{38}H_{61}N_6O_4S_2^+$ (disulfide dimer + H^+), 729.4190; found, 729.4144.

Preparation of Inhibitor Stock Solutions. Each of the inhibitors (**1a**−**h**) was synthesized as a mixture of the corresponding two diastereomers. Analytical HPLC analysis indicated that the two diastereomers were present at approximately 1:1 ratio for all of the inhibitors, which were essentially free of other contaminants. Inhibitors **1a**−**d** were further purified into their pure diastereomers by reversed-phase HPLC equipped with a semipreparative C_{18} column,

which was eluted with a linear gradient of acetonitrile (20−35% in 45 min) in water plus 0.05% TFA (flow rate 5 mL/min). Inhibitors **1e**−**h**, which are more difficult to separate by HPLC, were used as mixtures of the two diastereomers. Typically, the stock solutions of inhibitors **1b**−**g** (2−3 mM) were prepared in 20 mM Mes buffer (pH 6.4), whereas **1a** and **1h** were dissolved in 95% ethanol. Prior to their use in enzymatic assays, all inhibitor solutions were treated with 4 mM TCEP for 3 h to ensure that they were in the free thiol form. For inhibition of cell growth, the inhibitor solutions were treated with 4 mM H_2O_2 for 12 h. This procedure resulted in their quantitative conversion into disulfide dimers as judged by mass spectrometry. Inhibitor concentrations (for **1a**−**g**) were determined by base hydrolysis to completion, followed by measuring absorbance at 405 nm. Stock solutions of inhibitor **1h** were prepared by weighing the desired amount of pure solid and dissolving in known volumes of ethanol.

Enzyme Inhibition Assays. Assay reactions (total volume of 1.0 mL) were carried out at room temperature in 50 mM potassium phosphate buffer (pH 7.0) containing 10 mM NaCl, 1.0 mM TCEP, 150 μM f-ML-*p*NA (30), *E. coli* Fe−PDF (23−238 ng/mL) or *B. subtilis* Co−PDF (78 ng/mL), and varying concentrations of inhibitor **1a**−**h**. The reactions involving Fe−PDF were allowed to proceed for 10 min before being quenched by the addition of 10 mM H_2O_2 (final concentration). The Co−PDF reactions were incubated for 30 min and terminated by heat inactivation for 5 min at 95 °C. After cooling to room temperature, the thiol inhibitors were chelated by treatment with 2 molar equiv of 4-chloromercuribenzoic acid for 5 min (many of the thiol inhibitors also inhibit the coupling enzyme). The resulting mixture was then incubated with 0.5−1 unit of *Aeromonas* aminopeptidase for 2−4 min, and the amount of released *p*-nitroaniline was determined by measuring absorbance at 405 nm (*30*). All of the inhibitors tested exhibit competitive inhibition.

To examine whether the observed inhibition was time-dependent, the reaction (1 mL) was carried out in the phosphate buffer (pH 7.0) containing 200 μM f-ML-*p*NA as substrate and 0−100 nM L-**1b**. After the reaction was initiated at time 0 by the addition of 78−780 ng of *B. subtilis* Co−PDF, 125-μL aliquots were withdrawn at 30-s or 5-min intervals and quenched with 10 μL of 10% trifluoroacetic acid. The pH of the resulting solution was adjusted back to neutrality with 10 N KOH and the thiol inhibitor was quenched with 10 μM 4-chloromercuribenzoic acid (final concentration). The amount of deformylase reaction was then determined by the aminopeptidase assay (*30*) as described above and plotted against reaction time.

Cell Growth Inhibition Studies. Overnight cultures of *B. subtilis* and *E. coli* were diluted 1000-fold into 5 mL of fresh Luria−Bertani (LB) medium containing inhibitor L-**1b** and grown at 37 °C. Cell densities (OD_{600}) were recorded at regular time intervals over a 4.5 h period. Diluted cell cultures (1000-fold) were also grown to mid-log phase (OD_{600} = 0.2) and treated with L-**1b**, and cell were densities recorded over a 2.5 h period. All growth inhibition experiments were done in triplicate with inhibitor solutions that had been preincubated with hydrogen peroxide.

Determination of Minimal Inhibitory Concentrations (MIC). Overnight bacterial cultures were diluted 100-fold into fresh LB medium and grown to OD_{600} = 0.1. The cell cultures were again diluted by 100-fold into fresh LB medium containing serial dilutions (2-fold) of the thiol inhibitors **1a**−**h**. For *B. subtilis*, *S. epidermidis*, and *E. faecalis*, cells (1 mL/tube) were incubated at 37 °C in 15-mL culture tubes and shaken at 50 rpm for 5−20 h. *E. coli* cells were grown at 37 °C in agitated 96-well microtiter plates placed in a humidified incubator for 13 h (100 μL/well). Cell densities (OD_{600}) were recorded on an automated plate reader for *E. coli* cells or on a UV−vis spectrophotometer for all other cells. The MIC value is defined as the lowest inhibitor concentration that results in ≥99.9% growth inhibition. Data reported represent the mean ± SD from at least three independent sets of experiments.

RESULTS AND DISCUSSION

Design and Synthesis of PDF Inhibitors. We have previously found that a dipeptide, *N*-formylmethionylleucyl-*p*-nitroanilide (f-ML-*p*NA), is a particularly potent substrate due to its high affinity (K_M = 20 μM) for the PDF active site (30). We subsequently synthesized a tetrahedral transition-state analogue, (*S*)-2-*O*-(*H*-phosphonoxy)-L-caproyl-L-leucyl-*p*-nitroanilide (PCLNA), which acts as a weak competitive inhibitor of *E. coli* PDF (K_I = 37 μM) (*31*). X-ray crystallographic analysis of the PDF−PCLNA complex reveals that one of the phosphonate oxygens is directly ligated to the catalytic metal ion, replacing the metal-bound water (*24*). We reasoned that change of the phosphonate into a thiol group (compound **1**) (Figure 1) should increase the inhibitor potency, because sulfur is a superior ligand for transition metals such as Fe^{2+} over oxygen. Peptide thiols have previously been shown to be highly effective inhibitors of Zn^{2+} metallopeptidases (*32*−*34*).

Synthesis of inhibitor **1** is outlined in Figure 1. 2-Alkylacrylic acid **4** was synthesized from dimethyl malonate in four steps according to a literature procedure (*26*−*29*). Conjugate addition of thiolacetic acid to acid **4** gave 3-(*S*-acetyl)mercapto-2-alkylpropionic acid **5** (*33*). Acid **5** was coupled to amine **7** with DCC to give thioester **8**. Reduction of thioester **8** with $NaBH_4$ and removal of the Boc group with TFA (for **1b**−**h**) afforded the desired inhibitor **1** as a mixture of two diastereomers, which differ in stereochemistry (*R* vs *S* configuration) at the α-position of their P_1' residue. HPLC analysis revealed a ∼1:1 ratio of the two diastereomers for all of the inhibitors. Pure diastereomers of inhibitors **1a**−**d** were obtained by preparative HPLC. The other inhibitors (**1e**−**h**) were used in this work as mixtures of the two stereoisomers (due to difficulty in their preparative separation).

Inhibition of PDF Enzyme. Kinetic characterization was performed for the HPLC purified diastereomers of inhibitors **1a**−**d** and the diastereomeric mixtures of **1e**−**h**. Figure 2A shows a typical Lineweaver−Burk plot for the hydrolysis of f-ML-*p*NA by *E. coli* PDF in the presence of varying concentrations of inhibitor L-**1a**, in which the P_1' residue has an *n*-butyl side chain (R_1 = *n*-butyl) in the *S* configuration. Data fitting gave an inhibition constant (K_I) of 55 nM for L-**1a**. The other diastereomer, D-**1a**, is 12-fold less potent, with a K_I value of 650 nM (Table 1). Among the inhibitors we have synthesized, inhibitor L-**1b** is most potent against *E. coli* PDF (K_I = 19 nM) (Table 1). The other diastereomer (D-**1b**) is also a relatively potent inhibitor (K_I = 170 nM).

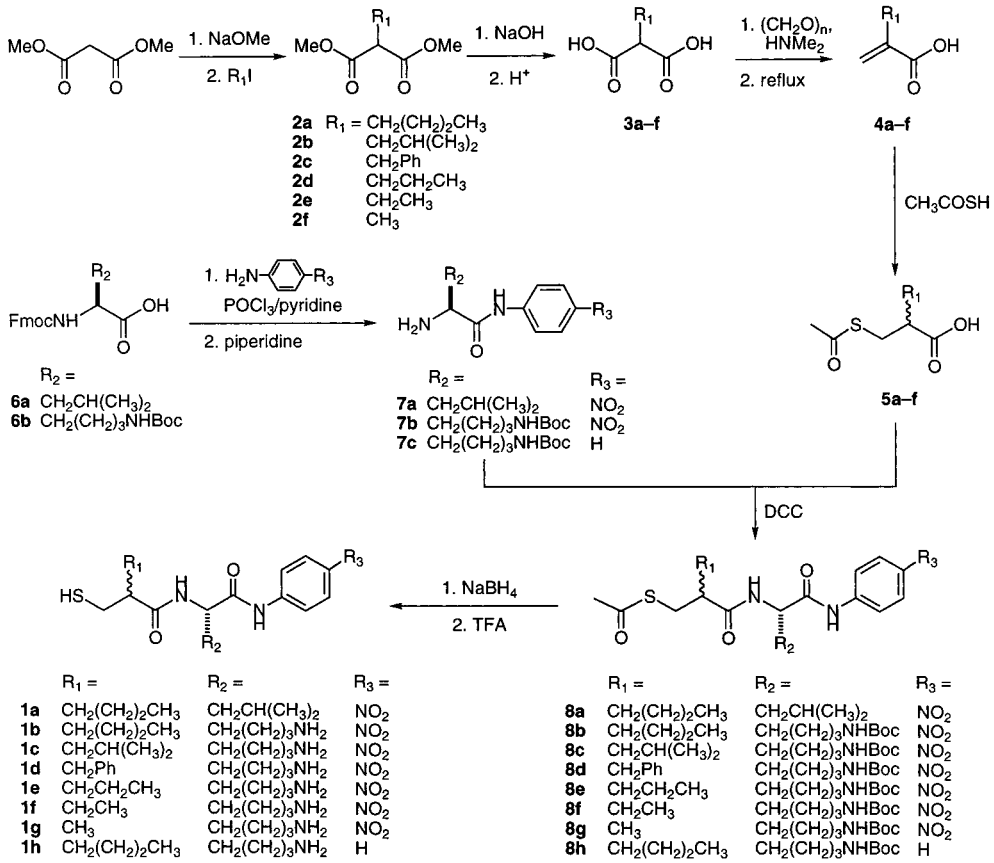

FIGURE 1: Structure and synthesis of inhibitors **1a**−**h**.

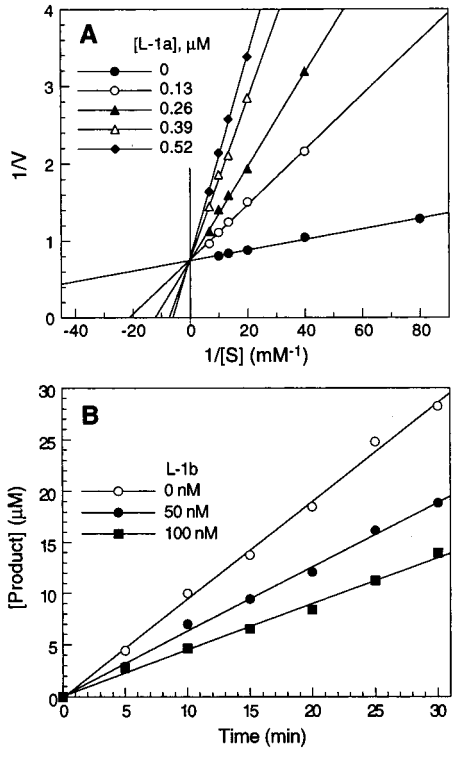

FIGURE 2: (A) Lineweaver−Burk plot of hydrolysis of f-ML-*p*NA by *E. coli* Fe−PDF in the presence of indicated amounts of inhibitor **1a**. Data were fitted against the Michaelis−Menten equation. (B) Time courses for the hydrolysis of f-ML-*p*NA (200 μM) by *B. subtilis* Co−PDF in the presence and absence of inhibitor L-**1b**.

To examine whether the observed inhibition is time-dependent (e.g., slow-binding inhibition), the reaction time course of *B. subtilis* Co−PDF in the presence or absence of L-**1b** was monitored over 30 min; a straight line was produced in each case (Figure 2B). Therefore, we conclude that **1a** and **1b** are simple competitive inhibitors. Because of their structural similarity, **1c**−**h** should also act as competitive inhibitors and their inhibitory behavior as determined at a minimum of five different inhibitor concentrations was indeed consistent with the competitive inhibition model. Our assignment of the more potent isomer as having the L (*S*) configuration at the P_1' site is based on the following observations: (1) *N*-formyl-D-methionyl peptides are not PDF substrates (*10*) and (2) the phosphonate inhibitor

Table 1: Inhibition Constants (K_I) and MIC Values for **1a**−**h**[a]

	E. coli		*B. subtilis*	
inhibitor	K_I (nM)	MIC (μM)	K_I (nM)	MIC (μM)
L-**1a**	55 ± 3	≫100	ND	≫100
D-**1a**	650 ± 60	ND	ND	ND
L-**1b**	19 ± 1	75−100	11 ± 1	6.4 ± 1.5
D-**1b**	170 ± 21	>100	293 ± 40	13 ± 3
1c	670 ± 70	38−100	93 ± 8	10 ± 2
L-**1c**	380 ± 38	ND	46 ± 3	ND
D-**1c**	13 400 ± 1000	ND	590 ± 50	ND
1d	310 ± 23	>100	95 ± 16	5.1 ± 1.1
L-**1d**	190 ± 20	ND	74 ± 9	ND
D-**1d**	415 ± 29	ND	1100 ± 60	ND
1e	798 ± 115	~120	84 ± 13	18 ± 3
1f	14 200 ± 2400	>120	1040 ± 160	60 ± 5
1g	15 700 ± 5300	≫100	3090 ± 430	150 ± 24
1h	264 ± 32	175 ± 22	73 ± 14	50 ± 5

[a] Data reported are mean ± SD for a minimum of three experiments. MIC values refer to monomer concentrations, although all growth inhibition experiments were carried out with the dimer forms and **1c**−**h** were used as mixtures of two diastereomers. ND, not determined.

PCLNA with its P_1' residue in the L configuration is more potent than the corresponding D-isomer (*31*). However, this assignment should be regarded as tentative until confirmed by X-ray crystallography (which is already in progress).

The identity of the P_1' side chain is critical for high-affinity binding to the PDF active site. Truncation of the *n*-butyl side chain of **1b** to a methyl group caused nearly 10^3-fold reduction in affinity for the *E. coli* enzyme (K_I = 15.7 μM for **1g**). Shortening the P_1' side chain by one and two methylene groups also decreased the potency by ~40- and 750-fold, respectively (K_I = 798 nM for **1e** and 14.2 μM for **1f**). Even a minor change from the *n*-butyl group to isobutyl group resulted in a 20-fold decrease in affinity (K_I = 380 nM for L-**1c**). A benzyl group is, however, relatively well tolerated at this position (K_I = 190 nM for L-**1d**). PDF is known to strongly prefer a methionine or norleucine, and to a lesser extent a phenylalanine, at the P_1' position of a substrate (*10*, *35*, *36*). It appears that the S_1' pocket prefers an unbranched side chain, which can readily bend into a curved conformation, as observed in the X-ray crystal structure (*24*). The benzene ring of phenylalanine apparently provides a reasonable mimic of the bent side chain. Another key element for high-affinity binding to PDF active site is the presence of a *p*-nitroanilide group. Inhibitor **1h** (K_I = 264 nM), which lacks the *p*-nitro group but is otherwise identical to inhibitor **1b**, is an order of magnitude less potent than **1b**. We have previously shown that removal of the *p*-nitroanilide group from f-ML-*p*NA (K_M = 20 μM) decreases its affinity for *E. coli* PDF by 40-fold (K_M = 800 μM for f-ML-NH_2) (*30*). Simple deletion of the *p*-nitro group also causes >20-fold increase in the K_M value (*37*). X-ray crystal structure shows that the *p*-nitro group is engaged into specific hydrogen-bonding interactions with enzyme active-site residues (*24*). Finally, the identity of the P_2' side chain can have some effect on the overall binding affinity. Inhibitors **1a** and **1b** only differ at this position but have a 3-fold difference in affinity (Table 1). In the crystal structure, the P_2' side chain is involved in hydrophobic interactions with the protein but is mostly exposed to the solvent (*24*). It is expected that amino acids with amphipathic side chains (e.g., lysine and arginine) would be most preferred at this position by the enzyme, as their nonpolar portion can favorably interact with the hydrophobic protein surface while their hydrophilic end groups (e.g., amine and guanidine) can interact with the polar solvent molecules.

Compounds **1a**−**h** are also highly potent against *B. subtilis* PDF; in fact, they are generally more potent against the *B. subtilis* enzyme (e.g., K_I = 11 nM for L-**1b**) than against the *E. coli* enzyme (K_I = 19 nM for L-**1b**). A similar decreasing trend in potency was observed when the P_1' side chain was changed from *n*-butyl to other functional groups or when the *p*-nitro group was removed, although the *B. subtilis* enzyme is somewhat more tolerant to changes in the P_1' side chain structure than the *E. coli* enzyme (Table 1).

The relatively small difference in K_I values for the L- vs D-diastereomers (L-**1d** and D-**1d** in particular) is worth some comments (Table 1). Cross-contamination due to imperfect separation on HPLC would undoubtedly result in an overestimate of the potency (lower K_I value) for the less active isomer, the D-isomers in this case. This contribution should be small, if any, since the two diastereomers of **1a**−**d** were quite well separated and the D-isomers were always the first

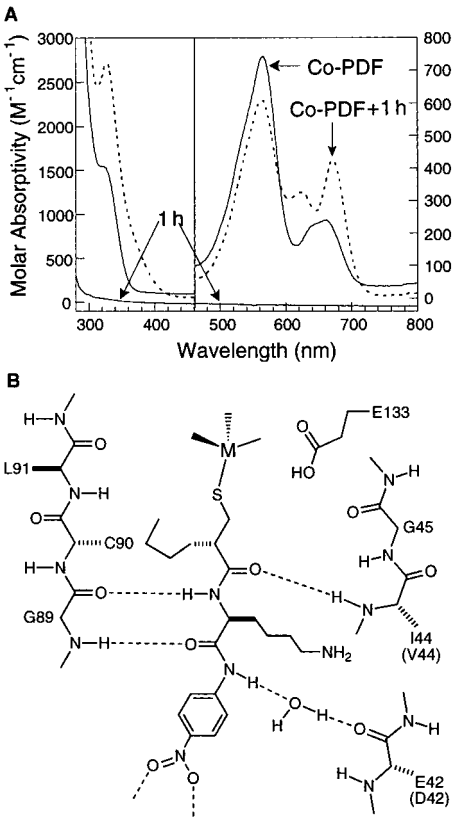

FIGURE 3: (A) Absorption spectrum of *E. coli* Co−PDF (95 μM) in the absence and presence of inhibitor **1h** (300 μM). (B) Proposed model for the hydrogen-bonding network between *E. coli* PDF and inhibitor L-**1b**. The corresponding residues in *B. subtilis*, when different from those of *E. coli* PDF, are shown in parentheses.

species to elute from the column (data not shown). Also, while L-**1d** and D-**1d** have only a 2-fold difference in K_I against *E. coli* PDF, the same inhibitor preparations exhibited a 15-fold difference in K_I toward the *B. subtilis* enzyme. A more likely explanation may be that the P_1' side chain of both diastereomers occupies the same S_1' binding pocket in PDF, while the relatively small mercaptomethyl group approaches the metal ion from two opposite orientations. We have previously observed that the two stereoselectively synthesized diastereomers of the phosphonate inhibitor PCLNA, which have opposite stereochemistry at their P_1' site, bind to *E. coli* PDF with only 3-fold difference in affinity (*31*). X-ray crystallographic study showed that their P_1' side chains of the two inhibitors indeed occupy the same binding pocket, whereas the phosphonate groups were ligated to the metal in two different orientations (B. Hao, W. Gong, M. K. Chan, and D.P., unpublished results).

Mechanism of Inhibition. The mechanism of inhibition was investigated with cobalt(II)-substituted *E. coli* PDF, which is structurally indistinguishable from Fe−PDF and has nearly wild-type activity (*18*, *24*). Because the spectroscopic properties of Co^{2+} ion are very sensitive to both the identity and the symmetry of its ligands, substitution of Co^{2+} for the native metal in a metalloenzyme provides a useful probe of the enzyme active-site environment (*38*). Figure 3A shows the electronic absorption spectra of the Co(II)-substituted *E. coli* PDF in the presence and absence of inhibitor **1h** (the *p*-nitroanilide group in other inhibitors has strong absorption at 350 nm, complicating the interpretation of their spectra). Co−PDF has an intense absorption at 325 nm (ϵ ~ 1500

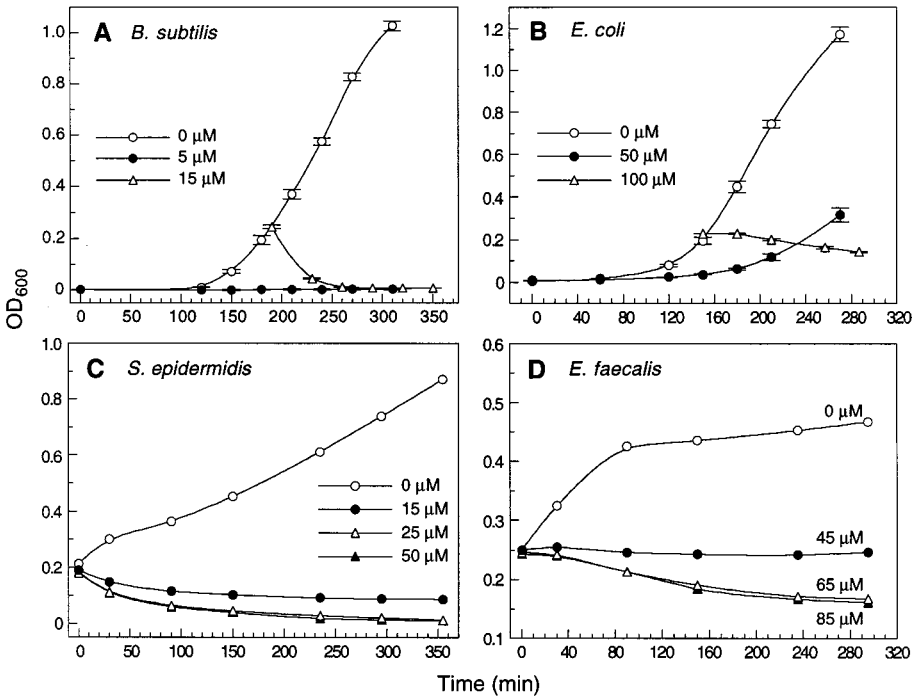

FIGURE 4: Inhibition of bacterial cell growth by **1b**. (A) *B. subtilis* growth curves. (○) No inhibitor; (●) 5 μM L-**1b** added to a freshly diluted culture (time 0); (△) 15 μM L-**1b** added at the exponential phase ($OD_{600} \sim 0.2$). (B) *E. coli* growth curves. (○) No inhibitor; (●) 50 μM L-**1b** added to a freshly diluted culture; (△) 100 μM **1b** added at the exponential phase. (C) *S. epidermidis* growth curves. (D) *E. faecalis* growth curves. In panels C and D, the specified concentrations of **1b** were added to cells at the exponential phase.

M^{-1} cm^{-1}), due to ligand-to-metal charge transfer from cysteine 90 to the Co^{2+}. In the visible region, PDF exhibits three bands at 565, 640, and 660 nm, which can be attributed to Co(II) d−d transitions. Binding of inhibitor **1h** resulted in a 2-fold increase in the intensity for the charge-transfer band and both red shift and intensity increase for the d−d bands (Figure 3A). These results indicate that the inhibitor thiol group is directly ligated to the metal ion upon inhibitor binding to the enzyme active site.

On the basis of the spectroscopic data and the crystal structure of the PDF−PCLNA complex (*24*), we propose the following working model for the interaction between inhibitor L-**1b** and PDF (Figure 3B). The inhibitor binds in an extended conformation, and together with β-strands IV and V from the protein, form an antiparallel β-sheet. The thiol group is directly ligated to the metal, replacing the bound water molecule. The *n*-butyl side chain of the P_1' residue occupies the deep hydrophobic S_1' pocket, whereas the P_2' lysyl side chain is pointing into the solvent. There is an extensive network of hydrogen bonds between the protein and the inhibitor, all of which are formed between the backbone carbonyls and amide protons. The carbonyls of the P_1' and P_2' residues of the inhibitor are engaged into hydrogen-bonding interactions to the amide protons of Ile-44 (Val-44 in *B. subtilis*) and Gly-89 of the protein, respectively. The amide proton of the inhibitor P_2' residue is hydrogen-bonded to the backbone carbonyl of Gly-89. The amide proton of the anilide group is hydrogen-bonded to Glu-42 (Asp-42 in *B. subtilis*) backbone carbonyl through a water molecule. The protein residue(s) that interacts with the nitro group is yet to be identified, because the crystal structure was complicated by the formation of a symmetry-related PDF dimer in the crystal (*24*). The aromatic ring of the anilide group is also involved in hydrophobic interactions with the protein surface. The predominant use of backbone elements in inhibitor binding is consistent with our observation that **1b**−**h** are effective inhibitors against both *E. coli* and *B. subtilis* enzymes, which share only 44% sequence identity (*25*).

Bacterial Cell Growth Inhibition. Inhibitor **1a** was initially synthesized and found to be a potent PDF inhibitor in vitro (K_I = 55 nM against *E. coli* PDF for L-**1a**). Unfortunately, it had little antibacterial activity when tested against either *E. coli* or *B. subtilis* cells. We felt that the lack of antibacterial activity could be due to poor membrane permeability and/or binding to other nonessential targets, among other factors (see below). We next synthesized inhibitor **1b**, in which a lysyl residue is substituted for the leucyl residue of **1a**. Our rationale was that (1) the presence of a polar amino group would increase the aqueous solubility of the inhibitor and therefore reduce nonspecific binding to lipophilic targets, and (2) the amino group might improve its membrane permeability since many clinically used antibiotics contain aliphatic amines (e.g., rifampicin, erythromycin, puromycin, and streptomycin). Indeed, inhibitor L-**1b** (K_I = 19 nM against *E. coli* PDF) not only is a more potent inhibitor toward the purified enzyme than L-**1a** but also exhibits potent antibacterial activity. Addition of 5 μM L-**1b** (2.0 μg/mL) to freshly diluted *B. subtilis* cells (a Gram-positive bacterium) in Luria−Bertani (LB) medium resulted in total growth inhibition (Figure 4A). Experiments with serial dilutions of L-**1b** produced a minimal inhibitory concentration (MIC) of 6.4 ± 1.5 μM (Table 1). When 15 μM L-**1b** was added to *B. subtilis* cells that had been grown to the exponential phase ($OD_{600} \sim 0.2$), complete cell lysis was observed after 2 h, as evidenced by the loss of optical density at 600 nm (Figure 4A). The drug-treated culture (1 mL) was then plated on LB agar plates and no colony was found after overnight incubation at 37 °C. The control cells, which were not treated with L-**1b**, produced $\sim 1 \times 10^9$ colony-forming units/mL of

culture. These results demonstrate that L-**1b** is a bactericidal agent to *B. subtilis* and the frequency of L-**1b**-resistant *B. subtilis* mutants is $<1 \times 10^{-9}$.

Interestingly, when 7 mM tris(2-carboxyethyl)phosphine (TCEP) was added into the growth medium to prevent the oxidation of the free thiol in L-**1b**, its antibacterial activity was nearly abolished. Addition of 7 mM TCEP alone to the medium had no effect on cell growth. Prior oxidation of L-**1b** into the disulfide-linked dimer with H_2O_2 further improved its antibacterial activity. Since the dimer does not inhibit PDF in vitro, we propose that dimerization of L-**1b**, which occurs spontaneously in the growth medium, increases its membrane permeability. Upon entering the cytoplasm, the dimer is reduced by cellular reductants to the free thiol form (*39*), which binds and inhibits the intracellular PDF. All of the MIC values reported in this work were obtained with preformed disulfide-linked inhibitor dimers.

Inhibitor **1b** (a ~1:1 mixture of L and D diastereomers) was also tested against two other Gram-positive bacteria, *Staphylococcus epidermidis* and *Enterococcus faecalis*, and Gram negative *E. coli*. *E. faecalis*, a common pathogen for endocarditis and urinary tract, wound, intraabdominal, and pelvic infections, has developed high-level resistance to β-lactams, aminoglycosides, and vancomycin (*1*, *40*). *S. epidermidis* has also become a significant pathogen responsible for many hospital-acquired infections and has been noted for resistance to several classes of antibiotics such as β-lactams, methicillin, aminoglycosides, and fluoroquinolones (1). Inhibitor **1b** is active against all three organisms (Figure 4B−D). The MIC values for *S. epidermidis* and *E. faecalis* are 18 ± 2 and 37 ± 3 μM, respectively. Furthermore, both *S. epidermidis* and *E. faecalis* were lysed when **1b** (25 and 65 μM, respectively) was added to their exponential-phase cultures (Figure 4C,D). Compound **1b** also inhibited the growth of *E. coli* cells, although higher doses were required (MIC = 75−100 μM for L-**1b**). When added to the freshly diluted culture (50 μM L-**1b**), it caused a pronounced delay in the cell growth (Figure 4B). When 100 μM **1b** was added to *E. coli* cells in the exponential phase, complete inhibition of cell growth was achieved (Figure 4B). A small decrease in optical density was observed over a 2-h period, indicating that **1b** is also capable of lysing Gram-negative bacteria. The higher MIC value is likely due to poorer transport of the inhibitor into Gram-negative cells, although other factors (e.g., drug efflux and degradation) could also be operative.

Correlation between MIC and K_I Values. To determine whether PDF is the molecular target responsible for the antibacterial activity of inhibitor **1b**, we synthesized a series of analogues of **1b** (compounds **1c**−**h**) (Figure 1). These inhibitors were deliberately designed to have reduced and varying degrees of potency against the PDF enzyme. Indeed, **1c**−**h** exhibit a wide range of K_I values, from 73 nM (**1h**) to 3.1 μM (**1g**), against *B. subtilis* PDF (Table 1). These inhibitors were then tested for inhibition of *B. subtilis* growth, and their MIC values were determined (Table 1). Plot of the MIC values against the K_I values revealed a linear correlation between the two, consistent with the notion that PDF is the molecular target of **1b**−**h** (Figure 5). Note that inhibitor **1h**, which differs from other inhibitors by lacking a C-terminal nitro group, is a relatively potent inhibitor against the purified enzyme (K_I = 73 nM) but showed relatively poor antibacterial activity (MIC = 50 μM), and thus resulting in significant deviation of the data point from the straight line. Likewise, L-**1a** is a very potent inhibitor but had no detectable antibacterial activity. The precise reason(s) behind the poor antibacterial activity of **1a** and **1h** remains to be determined, but there are several possible factors. First, **1a** and **1h** may be poorly transported through the cell membrane(s). Second, **1a** and **1h** may bind to other nonessential targets in the cell, rendering them less accessible to PDF. Indeed, **1a** and **1h**, due to their lack of the amino and nitro groups (Figure 1), respectively, are significantly more lipophilic than the other inhibitors and therefore more likely to bind to hydrophobic target molecules (e.g., proteins and membrane lipids). Other possibilities include poor stability in the bacterial cell and recognition by the active efflux systems (*41*). We have not obtained any analogues that have potent antibacterial activity but that do not inhibit the purified PDF. It is worth mentioning that PDF is a relatively abundant enzyme in bacterial cells. For example, an *E. coli* cell contains approximately 1300 PDF molecules (*17*), corresponding to a concentration of ~1.5 μM. Thus, regardless of how tightly an inhibitor may bind to PDF, the intracellular inhibitor concentration must be ≥1.5 μM in order to saturate all of the PDF enzymes.

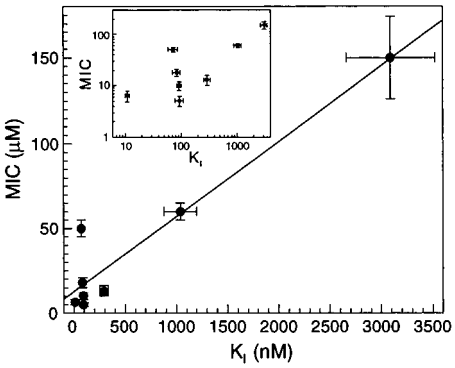

FIGURE 5: Relationship between inhibition constants (K_I) and MIC values for PDF inhibitors **1b**−**h**. (Inset) Plot of the same data in the logarithmic form. Error bars indicate the standard deviation for data from a minimum of three independent experiments.

How does inhibition of PDF lead to cell lysis? Since PDF deformylates essentially all of the polypeptides in a bacterial cell under normal growth conditions, blocking PDF function would result in N-terminally formylated proteins. Although many proteins are likely to function properly with the N-formyl group retained, some other protein(s) will certainly not be functional, due to either structural changes in the protein(s), inability to be further processed by downstream enzymes such as methionine aminopeptidase (8), or inability to fold correctly or be transported to the correct cellular location (e.g., periplasm). If one of the crucial enzymes involved in cell wall synthesis is among the protein(s) affected by loss of PDF activity, then cell lysis would ensue. Further experiments are already underway to address this question.

CONCLUSION

We have rationally designed and synthesized a series of potent, specific inhibitors for PDF. These represent the most potent PDF inhibitors that have been reported to date. These inhibitors exhibit moderate to potent antibacterial activity

toward both Gram-positive and Gram-negative bacteria and are bactericidal. We have previously found that the enzyme active site is formed by highly conserved residues (*24*). Binding of our inhibitors to PDF is primarily mediated by interactions with the protein backbone of these conserved residues. Thus, mutations in the PDF sequence are less likely to disrupt the inhibitor binding (without severely compromising its enzymatic activity). Indeed, although the inhibitors were originally designed based on the *E. coli* enzyme structure and the PDFs from *E. coli* and *B. subtilis* share only 44% sequence identity (*25*), they are nonetheless highly active toward both enzymes. Furthermore, the inhibitors are active antibiotics against all four bacterial organisms we have so far tested. These results suggest that PDF inhibitors designed to interact with these conserved residues (especially the backbone portion) will likely act as broad-spectrum antibiotics. The ability of these inhibitors to rapidly kill bacterial cells will make it more difficult for the cells to develop drug resistance.

NOTE ADDED IN PROOF

While this work was in press, Chen et al. (*42*) reported that PDF is the molecular target of actinonin, a naturally occurring antibacterial agent.

ACKNOWLEDGMENT

We thank Professor Neil Baker for providing the bacterial strains used in this work and Mrs. Susan Hatcher for high-resolution mass spectrometric analysis.

SUPPORTING INFORMATION AVAILABLE

Nine figures showing HPLC analysis of sample purity for inhibitors **1b**−**h**. This material is available free of charge via the Internet at http://pubs.acs.org.

REFERENCES

1. Neu, H. C. (1992) *Science 257*, 1064−1073.
2. Davis, J. D. (1994) *Science 264*, 375−382.
3. Spratt, B. G. (1994) *Science 264*, 388−393.
4. Gold, H. S., and Moellering, R. C., Jr. (1996) *New Engl. J. Med. 335*, 1445−1453.
5. Mazel, D., Pochet, S., and Marliere, P. (1994) *EMBO J. 13*, 914−923.
6. Meinnel, T., and Blanquet, S. (1994) *J. Bacteriol. 176*, 7387−7390.
7. Kozak, M. (1983) *Microbiol. Rev. 47*, 1−45.
8. Meinnel, T., Mechulam, Y., and Blanquet, S. (1993) *Biochimie 75*, 1061−1075.
9. Rajagopalan, P. T. R., Yu, X. C., and Pei, D. (1997) *J. Am. Chem. Soc. 119*, 12418−12419.
10. Rajagopalan, P. T. R., Datta, A., and Pei, D. (1997) *Biochemistry 36*, 13910−13918.
11. Groche, D., Becker, A., Schlichting, I., Kabasch, W., Schultz, S., and Wagner, A. F. V. (1998) *Biochem. Biophys. Res. Commun. 246*, 342−346.
12. Adams, J. M. (1968) *J. Mol. Biol. 33*, 571−589.
13. Livingston, D. M., and Leder, P. (1968) *Biochemistry 8*, 435−443.
14. Takeda, M., and Webster, R. E. (1968) *Proc. Natl. Acad. Sci. U.S.A. 60*, 1487−1494.
15. Rajagopalan, P. T. R., and Pei, D. (1998) *J. Biol. Chem. 273*, 22305−22310.
16. Meinnel, T., Lazennec, C., and Blanquet, S. (1995) *J. Mol. Biol. 254*, 175−183.
17. Ragusa, S., Blanquet, S., and Meinnel, T. (1998) *J. Mol. Biol. 280*, 515−523.
18. Rajagopalan, P. T. R., Gremmie, S., and Pei, D. (2000) *Biochemistry 39*, 779−790.
19. Meinnel, T., Blanquet, S., and Dardel, F. (1996) *J. Mol. Biol. 262*, 375−386.
20. Chan, M. K., Gong, W., Rajagopalan, P. T. R., Hao, B., Tsai, C. M., and Pei, D. (1997) *Biochemistry 36*, 13904−13909.
21. Becker, A., Schlichting, I., Kabsch, W., Schultz, S., and Wagner, A. F. V. (1998) *J. Biol. Chem. 273*, 11413−11416.
22. Dardel, F., Ragusa, S., Lazennec, C., Blanquet, S., and Meinnel, T. (1998) *J. Mol. Biol. 280*, 501−513.
23. Becker, A., Schlichting, I., Kabsch, W., Groche, D., Schultz, S., and Wagner, A. F. (1998) *Nat. Struct. Biol. 5*, 1053−1058.
24. Hao, B., Gong, W., Rajagopalan, P. T. R., Zhou, Y., Pei, D., and Chan, M. K. (1999) *Biochemistry 38*, 4712−4719.
25. Mazel, D., Coic, E., Blanchard, S., Saurin, W., and Marliere, P. (1997) *J. Mol. Biol. 266*, 939−949.
26. Duhamel, P., Duhamel, L., Danvy, D., Monteil, T., Lecomte, J.-M., and Schwartz, J.-C. (1996) European Patent No. 0729936 A1.
27. Smith, E. M., Swiss, G. F., Neustad, B. R., Gold, E. H., Sommer, J. A., Brown, A. D., Chiu, P. J. S., Moran, R., Sybertz, E. J., and Baum, T. (1988) *J. Med. Chem. 31*, 875−885.
28. Neustad, B. R., Smith, E. M., Nechuta, T. L., Bronnenkant, A. A., Haslanger, M. F., Watkins, R. W., Foster, C. J., and Sybertz, E. J. (1994) *J. Med. Chem. 37*, 2461−2476.
29. Mimura, T., Nakamura, Y., Nishino, J., Sawayama, T., Komiya, K., Deguchi, T., Kita, A., Nakamura, H., and Matsumoto, J. (1992) *J. Med. Chem. 35*, 602−608.
30. Wei, Y., and Pei, D. (1997) *Anal. Biochem. 250*, 29−35.
31. Hu, Y.-J., Rajagopalan, P. T. R., and Pei, D. (1998) *Bioorg. Med. Chem. Lett. 8*, 2479−2482.
32. Cushman, D. W., Cheung, H. S., Sabo, E. F., and Ondetti, M. A. (1977) *Biochemistry 16*, 5484−5491.
33. Ondetti, M. A., Condon, M. E., Reid, J., Sabo, E. F., Cheung, H. S., and Cushman, D. W. (1979) *Biochemistry 18*, 1427−1430.
34. Huntington, K. M., Bienvenue, D. L., Wei, Y., Bennett. B., Holz, R. C., and Pei, D. (1999) *Biochemistry 38*, 15587−15596.
35. Hu, Y.-J., Wei, Y., Zhou, Y., Rajagopalan, P. T. R., and Pei, D. (1999) *Biochemistry 38*, 643−650.
36. Meinnel, T., Patiny, L., Ragusa, S., and Blanquet, S. (1999) *Biochemistry 38*, 4287−4295.
37. Wei, Y. (1999) Peptide Deformylase: Characterization and Antibacterial Drug Design. Ph.D. Thesis, The Ohio State University, Columbus, OH.
38. Maret, W., and Vallee, B. L. (1993) *Methods Enzymol. 226*, 52−71.
39. Boehm, J. C., Kingsbury, W. D., Perry, D., and Gilvarg, C. (1983) *J. Biol. Chem. 258*, 14850−14856.
40. Schouten, M. A., Voss, A., and Hoogkamp-Korstanje, J. A. A. (1999) *Antimicrob. Agents Chemother. 43*, 2542−2546.
41. Nikaido, H. (1994) *Science 264*, 382−388.
42. Chen, D. Z., Patel, D. V., Hackbarth, C. J., Wang, W., Dreyer, G., Young, D., Margolis, P. S., Wu, C., Ni, Z.-J., Trias, J., White, R., and Yuan, Z. (2000) *Biochemistry 39*, 1256−1262.

BI992452Y